X-Disciplinarity

Original Article

DOI: https://doi.org/10.63174/xdi-AXQK2254

Independent Control of Co-polarized and Cross-polarized Light Using Metasurface for Vector Vortex Beam Generation

https://doi.org/10.63174/xdi-AXQK2254

Received: 18 Feb 2025

Accepted: 28 Feb 2025

Published: 8 Mar 2025

Open Access

Shuai Wang[1], Lei Liu[1], Zhicheng Zhang[2,3], Zhen Liu[2], Xingting Zhang[1,*]

Abstract: We present a metasurface design for generating multi-channel vector vortex beams through simultaneous control of phase and polarization states. The metasurface consists of nested silicon nanopillars on a SiO_2 substrate, designed to operate at 800 nm wavelength. By implementing independent control of deflection phase, lens phase, and vortex phase for each channel, we achieve the generation of dual-channel vector vortex beams with different topological charges. Numerical simulations demonstrate successful generation of vector vortex beams in separate channels, with both identical (l = 1) and different (l = 1 and l = 2) topological charges. The simulation results show well-defined doughnut-shaped intensity profiles and precise polarization control for each channel at the focal plane, confirming our design's capability for complex beam manipulation in multiple channels.

1. Introduction

Optical metasurfaces, artificially engineered two-dimensional structures with subwavelength thickness, have revolutionized the field of optics through their extraordinary capabilities in manipulating electromagnetic waves [1–4]. These ultrathin structures provide unique advantages of compact size and flexible wavefront control through carefully designed subwavelength units[5–7]. Recent developments in phase control mechanisms, especially the combination of geometric and propagation phases, have opened new avenues for generating complex structured light fields, where precise control of polarization and phase distributions is crucial [8–12].

Among various applications, the manipulation of light's angular momentum through metasurfaces has attracted particular attention [13,14]. Light waves inherently possess both spin and orbital angular momentum (SAM and OAM), representing two distinct degrees of freedom for optical manipulation [5,15,16]. While SAM is associated with circular polarization states, OAM arises from helical phase fronts characterized by a phase factor $e^{il\varphi}$, where l represents the topological charge [15,17,18]. Vortex beams, carrying OAM with a phase singularity at the center, have become particularly attractive for applications in high-capacity optical communications and quantum information processing [19,20].

The combination of polarization control and OAM has led to growing interest in vector vortex beams (VVBs), which feature spatially varying polarization states across their transverse plane [21,22]. Unlike conventional scalar-polarized light, vector beams exhibit unique focusing properties and polarization distributions, including radially and azimuthally polarized beams[23,24]. The higher-order Poincaré sphere provides an elegant framework for describing these complex light states. Despite these advances, existing methods face challenges in achieving simultaneous control of multiple channels while maintaining independent manipulation of phase and polarization states [25,26].

In this work, we propose a novel metasurface design for generating multi-channel VVBs through independent control of phase and polarization states. Based on Jones calculus analysis, we demonstrate a metasurface consisting of silicon nanopillars on a SiO_2 substrate, operating at 800 nm wavelength. Through optimization of geometric parameters and rotation angles, we achieve independent control of the deflection phase, lens phase, and vortex phase for each channel. Our theoretical analysis and simulations validate the design's capability to generate dual-channel VVBs with different topological charges, offering new possibilities for advanced optical applications in communications and quantum information processing.

2. Theory and Methods

The theoretical foundation of our design is based on the fundamental properties of light as a transverse wave, where oscillations occur perpendicular to the propagation direction. For a comprehensive understanding of polarization control in metasurfaces, we first established the mathematical framework using Jones calculus.

For a monochromatic polarized light, its polarization state can be represented by a two-dimensional Jones vector:

$$E = \begin{bmatrix} E_x \\ E_y \end{bmatrix} = \begin{bmatrix} E_{0x} e^{i\varphi_x} \\ E_{0y} e^{i\varphi_y} \end{bmatrix} \quad (1)$$

where E_{0x}, E_{0y} represent the amplitude components and φ_x, φ_y denote the phases along x and y directions, respectively. When light passes through a polarization-altering device, the transformation can be described by a Jones matrix:

[1]Faculty of Fundamental Subject Teaching, Shandong Agriculture and Engineering University, Jinan,Shandong, 250100, P.R.China
[2]Machinery and Electronics.Engineering College,Shandong Agriculture and Engineering University, Jinan,Shandong, 250100, P.R. China
[3]Hongdian (Shandong) Digital Technology Co., Ltd, Jinan, Shandong Province, 250199
*Corresponding:Author: Jnzhangxt@163.com (X. Zhang)

$$T = \begin{bmatrix} T_{11} & T_{12} \\ T_{21} & T_{22} \end{bmatrix} \quad (2)$$

where T_{ij} are complex transmission coefficients. The output field can then be expressed as $E_{out} = T \cdot E_{in}$, where E_{in} and E_{out} represent the polarization states of incident and transmitted light, respectively.

For a birefringent unit structure exhibiting different responses along its principal axes, the Jones matrix without rotation is:

$$J = \begin{bmatrix} t_x e^{i\varphi_x} & 0 \\ 0 & t_y e^{i\varphi_y} \end{bmatrix} \quad (3)$$

where t_x t_y represent the transmission coefficients, and φ_x, φ_y are the phase delays along the x and y axes, respectively. When the unit structure rotates by an angle θ, the Jones matrix transforms according to:

$$J_\theta = R(-\theta)JR(\theta) \quad (4)$$

where $R(\theta)$ is the rotation matrix:

$$R(\theta) = \begin{bmatrix} \cos\theta & \sin\theta \\ -\sin\theta & \cos\theta \end{bmatrix} \quad (5)$$

For circularly polarized incident light ($E_L / E_R = (e_x \pm ie_y)/\sqrt{2}$), the output field becomes:

$$E_{out} = J_\theta E_{in}^{L/R} = \frac{t_x e^{i\varphi_x} + t_y e^{i\varphi_y}}{2} E_{in}^{L/R} + \frac{t_x e^{i\varphi_x} - t_y e^{i\varphi_y}}{2} e^{\pm 2i\theta} E_{in}^{R/L} \quad (6)$$

This equation reveals two crucial components: the co-polarized light maintaining the original polarization state and the cross-polarized light with an additional geometric phase ($\pm 2\theta$). The geometric phase can be continuously modulated from 0 to 2π by rotating the structure from 0 to π.

The transmission phase accumulation through the structure can be calculated as:

$$\varphi = \frac{2\pi}{\lambda} n_{eff} H \quad (7)$$

where n_{eff} is the effective refractive index, n_0 is the surrounding medium's refractive index, H is the structure height, and λ is the wavelength. By adjusting the geometric parameters of the unit structure, we can control the transmission phase while maintaining stable amplitude characteristics.

The theoretical foundation of our design stems from the fundamental properties of light as a transverse wave, where oscillations occur perpendicular to the propagation direction. This characteristic leads to light polarization, which can be precisely controlled through carefully designed optical elements. Our comprehensive theoretical framework enables independent control of both transmission phase and geometric phase, which is essential for generating high-quality VVBs. Most notably, the transmission coefficients depend only on the geometric parameters of the unit structure, ensuring amplitude stability regardless of rotation angle. Through careful design of the structural parameters and rotation angles of the metasurface elements, this framework allows for precise and independent control of both co-polarized and cross-polarized components, providing a robust platform for advanced wavefront manipulation.

The mechanism of optical metasurfaces is essentially based on the superposition of light fields. When incident light passes through the metasurface, it undergoes diffraction and subsequently interferes at the observation plane to form the desired image. To generate VVBs, we need to calculate the metasurface's effect on light using diffraction formulas, based on the phase and amplitude parameters of the target beam. The Rayleigh-Sommerfeld diffraction formula, which is a solution to the Helmholtz equation, is employed here:

$$U(x,y,d) = \frac{1}{i\lambda} \int_{-\infty}^{\infty} \int_{-\infty}^{\infty} U_0(x_0, y_0, 0) \frac{e^{ikr}}{r} \cos\theta dx_0 dy_0 \quad (8)$$

where $r = \sqrt{f^2 + (x - x_0)^2 + (y - y_0)^2}$ represents the distance between the object and image points, f is the distance between the object and image planes, and θ is the angle between the radius vector r from point $(x_0, y_0, 0)$ to (x, y, d) and the normal n at point $(x_0, y_0, 0)$. Through this diffraction formula, each unit structure on the metasurface contributes to the generation of the desired light field through Rayleigh-Sommerfeld diffraction and interference at the image plane. The collective behavior of these unit structures, with their specific arrangements, geometric dimensions, and rotation angles, enables precise control over both the phase and amplitude of the output light field.

From our previous theoretical analysis, we can deduce that a rotating birefringent unit structure can convert incident circularly polarized light into its orthogonal state while introducing a geometric phase. The output light consists of two components: the cross-polarized light carrying both geometric and transmission phases, and the co-polarized light maintaining its original polarization state with only transmission phase. In conventional geometric phase optical elements, the unconverted co-polarized light acts as noise, degrading the image contrast. To enhance the overall efficiency, we analyze the relationship between these two polarization states and develop a unit structure model capable of simultaneously controlling both components.

For a left-handed circularly polarized light incident on the birefringent structure, the Jones matrix can be expressed as[25]:

$$J = \begin{bmatrix} e^{i\varphi_{LL}} & e^{i(\varphi_{LR}+2\theta)} \\ e^{i(\varphi_{RL}-2\theta)} & e^{i\varphi_{RR}} \end{bmatrix} = \begin{bmatrix} e^{i\varphi_{LL}} & e^{i\varphi_{LR}} \\ e^{i\varphi_{RL}} & e^{i\varphi_{RR}} \end{bmatrix} \quad (9)$$

where φ_{LL} and φ_{RR} represent the transmission phases for co-polarized light, while φ_{LR} and φ_{RL} denote the cross-polarized components with geometric phase. Due to symmetry, we have $\varphi_{RR} = \varphi_{LL}$ and $\varphi_{RL} = \varphi_{LR}$. Through FDTD simulations, we investigated how the phase and amplitude of both polarization components vary with the rotation angle of the unit structure.

The general expression for simultaneous control of co-polarized and cross-polarized components can be derived as:

$$E_{out} = E_{co} + E_{cross} = \cos\frac{\varphi_x - \varphi_y}{2} e^{i\frac{\varphi_x + \varphi_y}{2}} E^{\frac{L}{R}} + \sin\frac{\varphi_x - \varphi_y}{2} e^{i\frac{\varphi_x - \varphi_y}{2}} e^{\pm i2\theta} E^{\frac{R}{L}} \quad (10)$$

where φ_x and φ_y represent the transmission phase delays in the x and y directions, respectively. The amplitudes of co-polarized and cross-polarized components are $T_{co} = cos(\Delta\varphi/2)$ and $T_{cross} = sin(\Delta\varphi/2)$, respectively, with their intensity ratio defined as $\eta = T_{cross} / T_{co}$. To achieve equal output power in both polarization channels, the phase difference $\Delta\varphi$ is set to $\pi/2$.

This formulation reveals the relationship between transmission phases in dif-

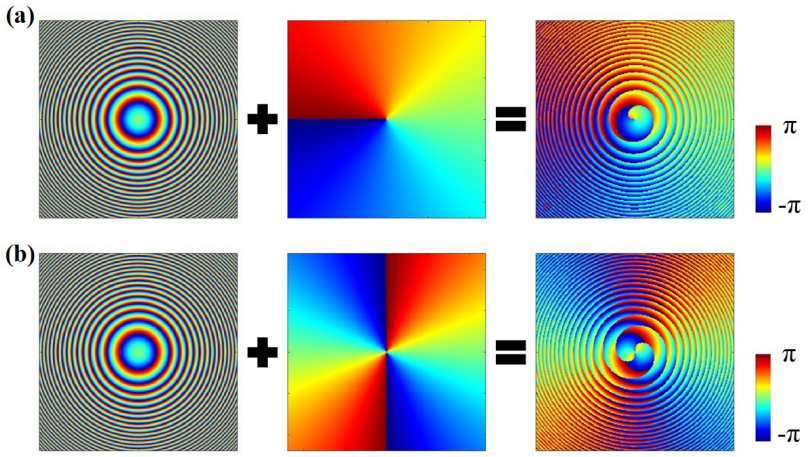

Figure 1 The phase distributions for topological charges of 1 (a) and 2 (b).

ferent polarization states and provides a theoretical foundation for independent control of both co-polarized and cross-polarized components through careful design of the nanoscale unit structure's geometric parameters and rotation angle.

3. Results and Discussion

To demonstrate the effectiveness of our design, we chose silicon (Si) as the material for nanopillars due to its high refractive index and low loss at the operating wavelength of 800 nm. The unit cell consists of a rectangular Si nanopillar on a square SiO_2 substrate. The phase delays in different directions were achieved by adjusting the length (L) and width (W) of the nanopillars. The structural parameters were optimized with a substrate period P of 380 nm and a nanopillar height H of 480 nm.

To validate our design, we implemented the metasurface using MATLAB for generating single-channel VVBs. The metasurface was designed with a square area of 76 μm × 76 μm, discretized into unit cells with dimensions of 0.38 μm × 0.38 μm. Under left-handed circularly polarized (LCP) light illumination at 800 nm wavelength, the metasurface was designed to impart both focusing and vortex phases, with a focal length of 60 μm and a topological charge of +1.

According to the principle of independent control of co-polarized and cross-polarized components derived in Equation (10), when LCP light $|L_{in}\rangle$ passes through the metasurface, it generates both co-polarized ($|L_{out}\rangle$) and

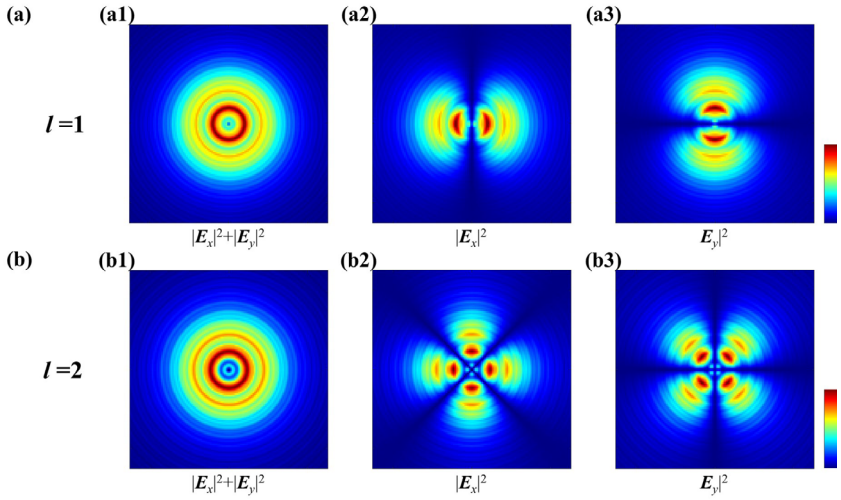

Figure 2 The intensity distribution of $|E_x|^2+|E_y|^2$, $|E_x|^2$ and $|E_y|^2$ of the VVB with the topological charge l = 1 (a) and l = 2 (b).

cross-polarized ($|R_{out}\rangle$) components. The co-polarized LCP component carries the transmission phase $\varphi_{L,r}$, while the cross-polarized RCP component carries both the transmission phase $\varphi_{R,r}$ and the geometric phase $\varphi_{\theta,r}$. The geometric phase introduced by the unit structure rotation is given by:

$$\varphi_{\theta,r} = 2\theta \tag{11}$$

where θ is the rotation angle of the unit structure. To generate VVBs, we require orthogonal circular polarizations with opposite topological charges. The phase for $\left|L_{out}\right\rangle$ is designed as:

$$\varphi_{L,out} = \varphi_{L,r} = \varphi_{focus} + \varphi_{Vor\_l=+1} \tag{12}$$

where φ_{Lens} represents the focusing phase and φ_{Vor}, l = +1 represents the vortex phase with topological charge +1. Similarly, the phase for $\left|R_{out}\right\rangle$ is:

$$\begin{aligned}\varphi_{R,out} &= \varphi_{R,r} + \varphi_{\theta,r} = \varphi_{R,r} + 2\theta \\ &= \varphi_{focus} + \varphi_{Vor\_l=-1}\end{aligned} \tag{13}$$

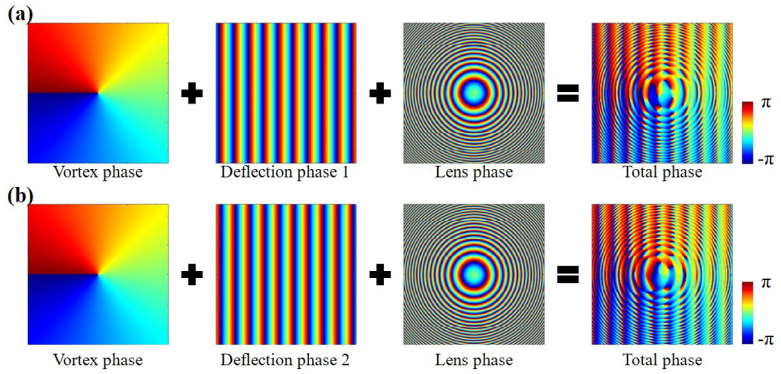

Figure 3 Phase of the metasurface for generating dual-channel VVBs whose topological charge is 1 with different deflection phase.

The geometric parameters and rotation angles of the metasurface unit structures were modulated according to Equations (12) and (13). The total phase distribution on the metasurface can be expressed as:

$$\varphi = \varphi_{Lens} + \varphi_{Vor} \tag{14}$$

The total phase of the vortex beam generated by the metasurface consists of lens phase and vortex phase, as shown in Figure 1(a) and (b) which display the phase distribution diagrams of vortex beams with topological charges of 1 and 2. This design enables simultaneous control of focusing and orbital angular momentum, which is essential for generating high-quality VVBs with specific topological charges.

We implemented the metasurface design using MATLAB, configuring both phase distribution and geometric parameters to generate VVBs. The metasurface was designed with dimensions $M \times N$ (where $M = N$) at the micrometer scale, with a focal length $f = 100$ μm. By incorporating both vortex and focusing phases, the metasurface functions as a quarter-wave plate to generate co-polarized and cross-polarized light components.

The simulation results for the first-order vector vortex beam (topological charge $l = 1$) at the focal plane are shown in Fig. 2(a1-a3). The total amplitude distribution (Fig. 2(a1)) reveals a characteristic doughnut-shaped intensity profile, while the x- and y- amplitude distributions (Fig. 2(a2-a3)) display complementary two-lobe patterns rotated 90° relative to each other. For the second-order vector vortex beam (topological charge $l = 2$), shown in Fig. 2(b1-b3), the total amplitude distribution exhibits a larger central dark core (Fig. 2(b1)), and the x- and y- components demonstrate four-lobe patterns (Fig. 2(b2-b3)) consistent with the higher topological charge.

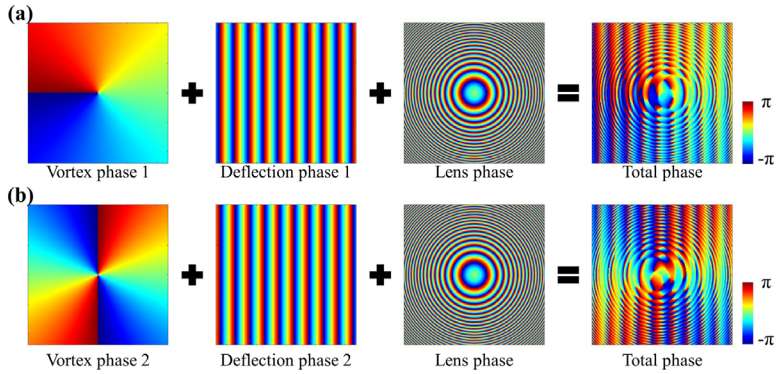

Figure 4 (a) Phase of the deflecting metasurface for generating vortex beam with topological charge 1 (a) and topological charge 2 (b).

The simulation results demonstrate the successful generation of VVBs through our metasurface design. The clear doughnut-shaped intensity profiles, well-defined polarization distributions, and symmetric patterns observed in both first and second-order beams confirm precise phase control and efficient polarization conversion at the focal plane.

To achieve multi-channel vector vortex beam generation, we designed a nested configuration of two metasurface sets. Each set was engineered with distinct deflection phases and independent vortex phases, enabling the generation of dual-channel beams with different topological charges. In each channel, the generated beams possess equal topological charges but opposite polarization states, which combine to form vector beams. The phase requirements for each metasurface set can be expressed as:

$$\begin{aligned} \varphi_1 &= \varphi_{Lens} + \varphi_{Vor\_l_1} + \varphi_{Def\_p_1} \\ \varphi_2 &= \varphi_{Lens} + \varphi_{Vor\_l_2} + \varphi_{Def\_p_2} \end{aligned} \tag{15}$$

The phase distributions for each metasurface set are illustrated in Fig. 3 and Fig. 4. Fig. 3 shows the phase profiles for generating dual-channel VVBs with identical topological charges ($l = 1$), where both (a) and (b) demonstrate the combination of deflection phase, lens phase, and vortex phase with $l = 1$. Fig. 4 presents the phase distributions for generating dual-channel VVBs with different topological charges ($l = 1$ and $l = 2$).

The simulation results at the focal plane for dual-channel VVBs with identical topological charges ($l = 1$) are presented in Fig. 5. The left and right channels each contain a vector vortex beam formed by the superposition of RCP light with topological charge $l = 1$ and LCP light with $l = -1$. The total amplitude distribution (Fig. 5(a)) and the corresponding x- (Fig. 5(b)) and y- (Fig. 5(c)) components clearly show two spatially separated vortex beams with characteristic intensity distributions.

For dual-channel VVBs with different topological charges ($l = 1$ and $l = 2$), the simulation results are shown in Fig. 6. The distinct doughnut-shaped patterns in the total amplitude distribution (Fig. 6(a)) and the corresponding polarization components (Fig. 6(b-c)) demonstrate successful generation of VVBs

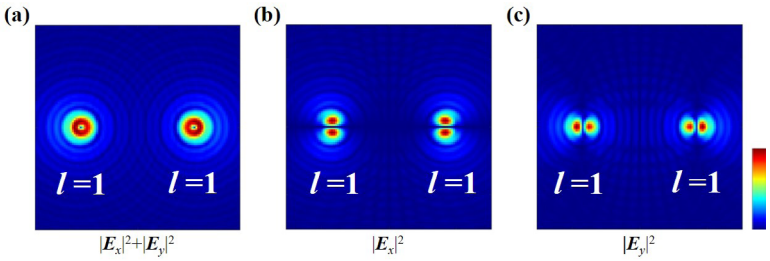

Figure 5 The intensity distribution of $|E_x|^2+|E_y|^2$, $|E_x|^2$ and $|E_y|^2$ of the dual-channel VVBs with $l = 1$.

with different topological charges in separate channels. The larger dark core in the $l = 2$ channel compared to the $l = 1$ channel confirms the expected behavior for higher-order vortex beams.

These results convincingly validate our design's capability to simultaneously generate and control multiple VVBs with independent topological charges and polarization states, demonstrating the versatility of our metasurface design for complex beam manipulation. Compared to conventional approaches using spatial light modulators or q-plates, our metasurface-based solution offers significant advantages in terms of device miniaturization, integration capability, and system stability. The demonstrated precise control over multiple channels makes our design particularly promising for practical applications. For example, in optical communication systems, the independent manipulation of multiple VVBs could enable high-capacity mode-division multiplexing, while in quantum information processing, it could facilitate the parallel manipulation of quantum states. Furthermore, our numerical simulations demonstrate that the design exhibits excellent wavelength adaptability, as it can be effectively extended to different spectral ranges by appropriately scaling the nanopillar geometric parameters. However, it should be noted that extending the design to larger arrays or shorter wavelengths may require careful consideration of fabrication challenges and potential coupling effects between adjacent structures.

4. Conclusion

In this work, we have demonstrated a novel metasurface design capable of generating multi-channel VVBs through the integration of nested phase control structures. The proposed design utilizes silicon nanopillars on a SiO_2 substrate, operating at a wavelength of 800 nm. Through careful optimization of the geometric parameters and phase distributions, we achieved independent control of deflection phase, lens phase, and vortex phase for each channel. The effectiveness of our design was validated through numerical simulations, successfully demonstrating dual-channel vector vortex beam generation with both identical and different topological charges. The simulation results showed well-separated channels with clear doughnut-shaped intensity profiles and precise polarization control at the focal plane. The distinct characteristics observed between first-order and second-order vortex beams in different channels confirm the excellent phase and polarization control capabilities of our design. Our proposed multi-channel metasurface design not only extends the functionality of conventional metasurfaces but also provides a promising platform for advanced applications in optical communications, multiplexing systems, and quantum information processing. Specifically, the demonstrated ability to independently control multiple VVBs can enable high-capacity optical communication systems through mode-division multiplexing, enhance the security of quantum key distribution protocols, and facilitate the implementation of quantum computing algorithms requiring multiple quantum states. The flexibility and precision of our design make it particularly suitable for next-generation optical information processing systems requiring simultaneous manipulation of multiple optical channels.

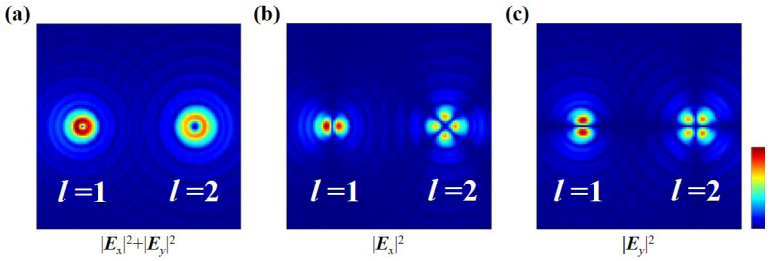

Figure 6 The intensity distribution of $|E_x|^2+|E_y|^2$, $|E_x|^2$ and $|E_y|^2$ of the dual-channel VVBs with $l = 1$ and $l = 2$.

Acknowledgements: This work is kindly supported by Shandong Provincial Natural Science Foundation (ZR2024QB360). We also gratefully acknowledge Shandong Agriculture and Engineering University Start-Up Fund for Talented Scholars (2024GCCZR-01, BSQJ202301).

Declaration of Competing Interest: The authors declare that they have no known competing financial interests or personal relationships that could have appeared to influence the work reported in this paper.

CrediT Authorship Contribution Statement: Shuai Wang: Investigation, Validation, Data curation, Writing original draft, Writing review & editing. Lei Liu, Zhicheng Zhang and Zhen Liu: Supervision, Conceptualization. Xinting Zhang: Supervision, Conceptualization, Funding acquisition, Resources, Writing-review & editing.

References

[1] S. Wan, K. Qu, Y. Shi, Z. Li, Z. Wang, C. Dai, J. Tang, Z. Li. "Multidimensional Encryption by Chip-Integrated Metasurfaces." *ACS Nano* **2024**, *18*, 28, 18693–700.

[2] B. Xiong, Y. Liu, Y. Xu, L. Deng, C.-W. Chen, J.-N. Wang, R. Peng, Y. Lai, Y. Liu, M. Wang. "Breaking the limitation of polarization multiplexing in optical metasurfaces with engineered noise." *Science* **2023**, *379*, 6629, 294–99.

[3] J. Zhao, X. Yu, X. Yang, Q. Xiang, H. Duan, Y. Yu. "Polarization independent subtractive color printing based on ultrathin hexagonal nanodisk-nanohole hybrid structure arrays." *Opt. Express* **2017**, *25*, 19, 23137–45.

[4] A. I. Kuznetsov, M. L. Brongersma, J. Yao, M. K. Chen, U. Levy, D. P. Tsai, N. I. Zheludev, A. Faraon, A. Arbabi, N. Yu, D. Chanda, K. B. Crozier, A. V. Kildishev, H. Wang, J. K. W. Yang, J. G. Valentine, P. Genevet, J. A. Fan, O. D. Miller, A. Majumdar, J. E. Fröch, D. Brady, F. Heide, A. Veeraraghavan, N. Engheta, A. Alù, A. Polman, H. A. Atwater, P. Thureja, R. Paniagua-Dominguez, S. T. Ha, A. I. Barreda, J. A. Schuller, I. Staude, G. Grinblat, Y. Kivshar, S. Peana, S. F. Yelin, A. Senichev, V. M. Shalaev, S. Saha, A. Boltasseva, J. Rho, D. K. Oh, J. Kim, J. Park, R. Devlin, R. A. Pala. "Roadmap for Optical Metasurfaces." *ACS Photonics* **2024**, *11*, 3, 816–65.

[5] W. Wang, L. Qi. "Light Management with Patterned Micro- and Nanostructure Arrays for Photocatalysis, Photovoltaics, and Optoelectronic and Optical Devices." **2019**, *29*, 25, 1807275.

[6] X. Luo, D. Tsai, M. Gu, M. Hong. "Subwavelength interference of light on structured surfaces." *Adv. Opt. Photon.* **2018**, *10*, 4, 757.

[7] X. Luo. "Subwavelength Artificial Structures: Opening a New Era for Engineering Optics." *Adv. Mater.* **2019**, *31*, 4, 1804680.

[8]Y. Yang, Y.-X. Ren, M. Chen, Y. Arita, C. Rosales-Guzmán. "Optical trapping with structured light: a review." *Adv. Photon.* **2021**, *3*, 3, 034001.

[9] Z. Huang, L. Cao. "Quantitative phase imaging based on holography: trends and new perspectives." *Light Sci. Appl.* **2024**, *13*, 1, 145.

[10] Z. S. Wan, H. Wang, Q. Liu, X. Fu, Y. J. Shen. "Ultra-Degree-of-Freedom Structured Light for Ultracapacity Information Carriers." *ACS Photonics* **2023**, *10*, 7, 2149-2164.

[11] J. Wang, K. Li, Z. Quan. "Integrated structured light manipulation." *Photonics Insights* **2024**, *3*, 3, R05.

[12] C. He, Y. Shen, A. Forbes. "Towards higher-dimensional structured light." *Light Sci Appl* **2022**, *11*, 1, 205.

[13] Y. Shi, Q. Song, I. Toftul, T. Zhu, Y. Yu, W. Zhu, D. P. Tsai, Y. Kivshar, A. Q. Liu. "Optical manipulation with metamaterial structures." *Applied Physics Reviews* **2022**, *9*, 3, 031303.

[14] H. Yang, P. He, K. Ou, Y. Q. Hu, Y. T. Jiang, X. N. Ou, H. H. Jia, Z. W. Xie, X. C. Yuan, H. G. Duan. "Angular momentum holography via a minimalist metasurface for optical nested encryption." *Light Sci. Appl.* **2023**, *12*, 1, 79.

[15] A. Forbes, L. Mkhumbuza, L. Feng. "Orbital angular momentum lasers." *Nat Rev Phys* **2024**, *6*, 6, 352–64.

[16] J. Chen, C. Wan, Q. Zhan. "Engineering photonic angular momentum with structured light: a review." *Adv. Photon.* **2021**, *3*, 6, 064001.

[17] M. Gu, C. Cheng, Z. Zhan, Z. Zhang, G. Cui, Y. Zhou, X. Zeng, S. Gao, D.-Y. Choi, C. Cheng, C. Liu. "Dielectric Supercell Metasurfaces for Generating Focused Higher-Order Poincaré Beams with the Residual Copolarization Component Eliminated." *ACS Photonics* **2024**, *11*, 1, 204–17.

[18] M. Gu, R. Zhang, C. Cheng, Q. Dong, X. Zeng, Y. Zhang, Z. Zhan, C. Liu, C. Cheng. "Metasurfaces for generating higher-order Poincaré beams by polarization-selective focusing and overall elimination of co-polarization components." *Opt. Express* **2023**, *31*, 23, 38921–38.

[19] S. H. Li, Q. Feng, H. X. Liu, J. Q. Han, Y. Shi, L. Li. "Aperture partitioning holographic metasurface for the generation of a directional vortex beam." *Opt. Express* **2024**, *32*, 26, 46290-46298.

[20] Y. Lian, X. Qi, Y. Wang, Z. Bai, Y. Wang, Z. Lu. "OAM beam generation in space and its applications: A review." *Optics and Lasers in Engineering* **2022**, *151*, 106923.

[21] X. Wang, Z. Nie, Y. Liang, J. Wang, T. Li, B. Jia. "Recent advances on optical vortex generation." *Nanophotonics* **2018**, *7*, 9, 1533–56.

[22] Y. Zhang, J. Gao, X. Yang. "Spatial variation of vector vortex beams with plasmonic metasurfaces." *Sci. Rep* **2019**, *9*, 1, 9969.

[23] J. Wang, Q. Jiang, D. Han. "A dielectric metasurface for controllable generation of tightly focused vector beams." *J. Phys. D: Appl. Phys.* **2023**, *56*, 39, 395106.

[24] M. Diouf, M. Harling, M. Yessenov, L. A. Hall, A. F. Abouraddy, K. C. Toussaint. "Space-time vector light sheets." *Opt. Express* **2021**, *29*, 23, 37225–33.

[25] M. Gu, L. Ma, G. Cui, Z. Zhang, Z. Zhan, Y. Zhou, S. Gao, D.-Y. Choi, C. Cheng, C. Liu. "Multichannel focused higher-order Poincaré sphere beam generation based on a dielectric geometric metasurface." *Opt. Express* **2024**, *32*, 11, 18958–71.

[26] Z. Zhang, M. Gu, G. Cui, Y. Zhou, Q. Dong, S. Gao, D.-Y. Choi, C. Cheng, C. Liu. "Manipulations of Vectorial-Structured Light by Spatially Interleaved Metasurfaces of Quarter-Wave-Plate Meta-Atoms." *J. Lightwave Technol.* **2024**, *42*, 19, 6863–73.